Report

Cell Systems

High-Throughput Microfluidic Labyrinth for the Label-free Isolation of Circulating Tumor Cells

Graphical Abstract

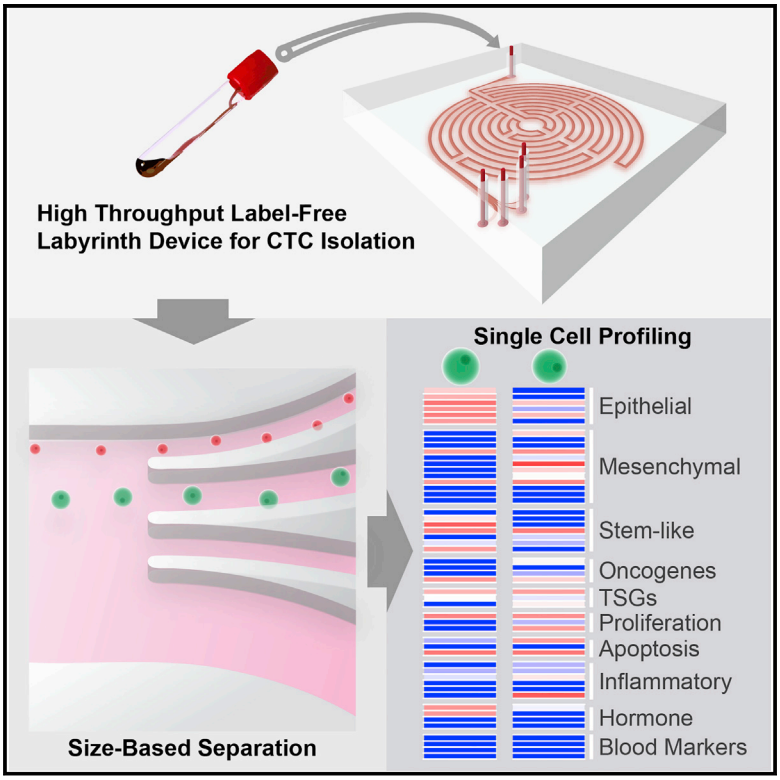

Highlights

- High-throughput label-free isolation of CTCs
- CTCs were isolated from 56 breast and 20 pancreatic cancer patients
- Unbiased molecular study of CTCs at the single-cell level
- 70 isolated single CTCs show both inter- and intra-patient molecular heterogeneity

Authors

Eric Lin, Lianette Rivera-Báez, Shamileh Fouladdel, ..., Ebrahim Azizi, Max S. Wicha, Sunitha Nagrath

Correspondence

mwicha@med.umich.edu (M.S.W.), snagrath@umich.edu (S.N.)

In Brief

High-throughput and label-free Labyrinth device that enables single CTC isolation and gene expression characterization.

Lin et al., 2017, Cell Systems 5, 295–304
September 27, 2017
http://dx.doi.org/10.1016/j.cels.2017.08.012

Cell Systems
Report

High-Throughput Microfluidic Labyrinth for the Label-free Isolation of Circulating Tumor Cells

Eric Lin,[1,4,6,7] Lianette Rivera-Báez,[1,4,6,7] Shamileh Fouladdel,[2,4,6,7] Hyeun Joong Yoon,[1,4,6] Stephanie Guthrie,[1,4,6] Jacob Wieger,[1,4,6] Yadwinder Deol,[2,4] Evan Keller,[2,4,6] Vaibhav Sahai,[2,4,6] Diane M. Simeone,[3,4,5] Monika L. Burness,[2,4] Ebrahim Azizi,[2,4,6] Max S. Wicha,[2,4,6,*] and Sunitha Nagrath[1,4,6,8,*]
[1]Department of Chemical Engineering, University of Michigan, Ann Arbor, MI 48109, USA
[2]Department of Internal Medicine, University of Michigan, Ann Arbor, MI 48109, USA
[3]Department of Surgery, University of Michigan, Ann Arbor, MI 48109, USA
[4]Translational Oncology Program, University of Michigan, Ann Arbor, MI 48109, USA
[5]Department of Molecular and Integrative Physiology, University of Michigan, Ann Arbor, MI 48109, USA
[6]Biointerfaces Institute, University of Michigan, Ann Arbor, MI 48109, USA
[7]These author contributed equally
[8]Lead Contact
*Correspondence: mwicha@med.umich.edu (M.S.W.), snagrath@umich.edu (S.N.)
http://dx.doi.org/10.1016/j.cels.2017.08.012

SUMMARY

We present "Labyrinth," a label-free microfluidic device to isolate circulating tumor cells (CTCs) using the combination of long loops and sharp corners to focus both CTCs and white blood cells (WBCs) at a high throughput of 2.5 mL/min. The high yield (>90%) and purity (600 WBCs/mL) of Labyrinth enabled us to profile gene expression in CTCs. As proof of principle, we used previously established cancer stem cell gene signatures to profile single cells isolated from the blood of breast cancer patients. We observed heterogeneous subpopulations of CTCs expressing genes for stem cells, epithelial cells, mesenchymal cells, and cells transitioning between epithelial and mesenchymal. Labyrinth offers a cell-surface marker-independent single-cell isolation platform to study heterogeneous CTC subpopulations.

INTRODUCTION

Multiple single-cell techniques have emerged in recent years, making the genome, transcriptome, and proteome of single cells accessible for detailed analyses. Such analyses could improve our understanding of both cancer biology and therapeutics, and facilitate insights into the metastatic process (Speicher, 2013). One of the strengths of single-cell technologies lies in their ability to interrogate rare cell events, such as in the detection of minimal residual disease or the analysis of circulating tumor cells (CTCs) in the peripheral blood (Krebs et al., 2014). Dawson et al. (2013) compared CTCs and primary tumor DNA from breast cancer patients by Next-Gen sequencing and suggested that CTCs are more informative for detecting secondary mutations than primary tumors. Yu et al. (2012) used single-cell RNA sequencing of CTCs from pancreatic cancer mouse models and identified the role of WNT signaling pathways in pancreatic cancer. However the exact composition and identity of CTCs remains an open question and resolving this may contribute to the detection of distinct drivers for metastasis. Previous studies have demonstrated that CTCs are highly enriched in the proportion of cells expressing cancer stem cell (CSC) markers compared with primary tumors from which they originated (Bednarz-Knoll et al., 2012; Yu et al., 2013a; Zhang et al., 2013). There is increasing evidence that tumor growth and metastasis is mediated by a subpopulation of tumor cells that display stem cell properties (Reya et al., 2001). These CSCs also mediate resistance to both conventional and molecularly targeted therapies (Brooks et al., 2015; Luo et al., 2015). Furthermore, recent studies have shown that CSCs exist in states indicative of epithelial-mesenchymal transition (EMT) or mesenchymal-epithelial transition (MET) (Sehl et al., 2015). However, investigating questions such as the relationship between CTCs and CSCs will require an evolution of single-cell profiling techniques to better probe the heterogeneity of CTCs.

Many microfluidic approaches rely on positive or negative selection to isolate CTCs. The most widely used method is immune-affinity capture with antibodies targeting molecules, such as the epithelial cell adhesion molecule (EpCAM), which are expressed exclusively on tumor cells and are absent in blood cells. This strategy has been successfully validated for use in prognosis, therapeutic monitoring, and molecular diagnosis (Maheswaran et al., 2008; Nagrath et al., 2007; Stott et al., 2010a, 2010b; Yu et al., 2013a). However, not all CTCs express EpCAM (Pantel and Speicher, 2016). Furthermore, downstream single-cell analysis is challenging due to the complex protocols (some of which might interfere with RNA stability) for releasing CTCs captured on the devices (Labib et al., 2016; Sheng et al., 2014; Yoon et al., 2016; Yu et al., 2013b).

In an attempt to move away from affinity-based isolation approaches, researchers have turned toward size-based technologies. CTCs derived from solid tumors are larger than the majority of cells in circulating blood (Jackson et al., 2017), making discrimination by size an attractive strategy for isolating CTCs, as demonstrated in studies that use filtration techniques

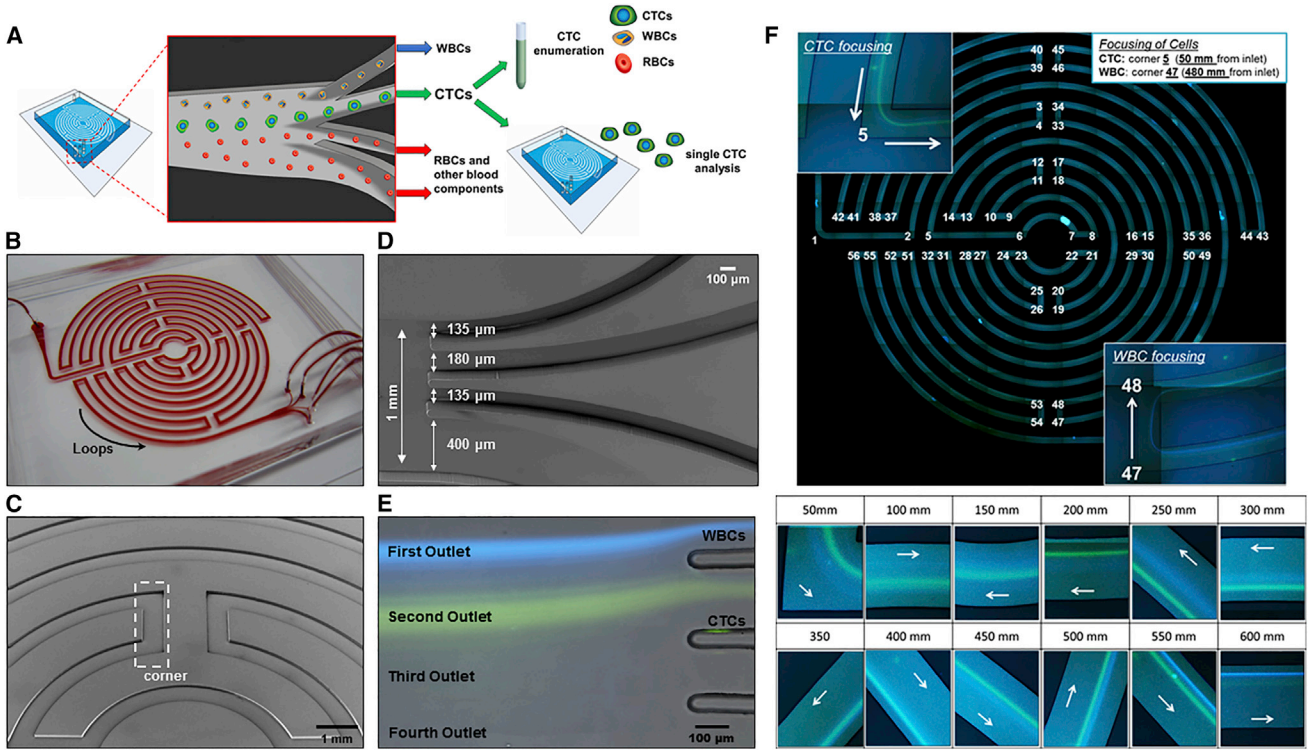

Figure 1. Device Design and Mechanism of Labyrinth

(A) Workflow of Labyrinth system. CTCs are separated through Labyrinth, and can be used for downstream analysis or further purified by applying second Labyrinth for single-cell analysis.

(B) Labyrinth loaded with red dye and the indication of "loops."

(C) SEM image of the outlet design.

(D) SEM image of the channel and the indication of "corners."

(E) The separation of labeled WBC/MCF-7 cell line into individual outlets.

(F) Focusing and separation of labeled WBCs and MCF-7 GFP cells along Labyrinth. Cancer cells are focused after traveling for 50 mm from inlet in Labyrinth, while WBCs are focused after 480 mm. Streams of cancer cells and WBCs are well separated at outlet.

to this end (Khoja et al., 2012; Lin et al., 2010; Paterlini-Brechot and Benali, 2007; Vona et al., 2004). The issues encountered with these approaches include pore clogging, high-pressure drop, pre-fixation to prevent CTC loss, low throughput, and excessive non-specific cell retention. Other label-free separation techniques reported in the literature include a deterministic lateral displacement separation method (Liu et al., 2013), a microfluidic flow fractionation approach (Hyun et al., 2013), and acoustic-based separation (Li et al., 2015). However, one of the common limitations among these techniques is the limited flow rate or yet to successfully isolate CTCs from clinical specimens. Recently, inertial migration of particles has been introduced and applied in various studies to achieve high-throughput particle separation based on particle size (Di Carlo et al., 2007). Sun et al. (2012), inspired by a single spiral channel, developed a double-spiral microchannel for label-free tumor cell separation and enrichment. Ozkumur et al. (2013) applied the inertial focusing in a relatively short sinusoidal channel, along with lateral displacement and immunomagnetic selection in the integrated microfluidic system known as the "CTC-iChip." Although this technology is promising, an unbiased molecular study of CTCs cannot be achieved where a manual selection of CTCs based on an EpCAM+/CD45– phenotype was required to overcome the limitation of insufficient purity (Karabacak et al., 2014). Hence, we developed a completely label-free and surface expression-independent microfluidic Labyrinth (Figure 1A) to isolate CTCs from blood cells with high recovery, while achieving the highest purity among all label-free technologies. The presented method identified CTC subpopulations entirely based on the genetic signature, without the need of manual selection based on either positive or negative protein expression, which were adopted in other label-free methods.

RESULTS

Labyrinth Design and Physical Principle of Separation

The design of our device is inspired by the Labyrinth in Greek mythology, an elaborate structure with numerous turns and corners built to hold the Minotaur. We applied a similar structure for the size-based enrichment of CTCs by bulk depletion of hematopoietic cells using inertial microfluidics-based separation.

Particle Focusing

The inertial microfluidics-based particle separation relies on the equilibrium between inertial lift forces and Dean flow, which

results in the migration of particles during laminar flow in microfluidic devices with curved channels (Figure S1). Particles in a straight channel experience stresses that act over the entire channel surface, including shear stress that yields drag forces and normal stress that yields lift forces perpendicular to the direction of flow. The migration of particles due to lift forces was first observed by Segré and Silberberg in the 1960s (Segré and Silberberg, 1961; Silberberg, 1962). Di Carlo et al. (2007) reported that particles would be maintained at specific positions due to the combination of inertial lift forces where shear gradient lift pushes the particles toward the wall and the wall lift effect pushes the particles toward the center (Stott et al., 2010b). These forces will confine the particles in a straight channel to several equilibrium positions, where the number of equilibrium positions is related to the geometry of the channel.

A relation describing the magnitude of lift force (F_z) was reported by ASMOLOV (1999):

$$F_z = \frac{\mu^2}{\rho} Re_p^2 f_c(\mathrm{Re}_c, x_c) \,, \qquad \text{(Equation 1)}$$

where Re_p is the particle Reynolds number, Re_c is the channel Reynolds number, and x_c is the position of the particle within the channel.

Particle Separation

The Dean flow, on the other hand, occurs in the flow in curved channels. Dean flow is secondary flow due to the centrifugal effects that will affect the particle equilibrium positions (Gossett and Carlo, 2009). Dean flow is characterized by counter-rotating vortices, where the flow at the midline of the channel is directed outward around a curve, while the flow at the top and bottom of the channel is directed inward (Gossett and Carlo, 2009). The drag force due to Dean flow (F_D) is correlated with the particle size and curvature of the channel, and this drag force will also affect the equilibrium position of the particles. Therefore, the equilibrium between inertial lift forces and the drag force from Dean flow can be utilized for size-based sorting (Sun et al., 2012).

In the presence of inertial lift forces that keep a particle in a stationary position, an expression of drag force F_D is raised by Di Carlo et al. (2007):

$$F_D \sim \rho U_m^2 a D_h^2 r^{-1} \,, \qquad \text{(Equation 2)}$$

where U_m is the maximum channel velocity, a is the particle diameter, D_h is the hydraulic diameter, and r is the radius of curvature of the channel.

The lift forces stabilize particles at positions located along the centerline of a channel cross-section, while Dean flow drag forces cause particles to migrate around the cross-section. A new equilibrium position can be estimated from the ratio of F_z to F_D (Di Carlo et al., 2007):

$$\frac{F_z}{F_D} = \frac{1}{\delta}\left(\frac{a}{D_h}\right)^3 \mathrm{Re}_c^n, \quad (n<0) \,, \qquad \text{(Equation 3)}$$

where δ is the curvature ratio,

$$\delta = \frac{D_h}{2r} \,. \qquad \text{(Equation 4)}$$

Cell Separation

CTCs can be isolated from other blood cells in curved microfluidic devices by focusing different sized cells into different streamlines and collecting them into individual outlet channels. The inertial force can be considered as the driving force that focuses the particles, while the drag force from Dean flow is the force that causes particle migration away from the center of the channel, leading to size-based separation (Figure S1).

Given the fact that F_z is proportional to the square of particle size (Equation 1), blood cells are more difficult to focus in microfluidic channels due to their smaller size compared with CTCs. It has been proposed that sharp curves enhance the focusing of smaller particles (Martel and Toner, 2013; Sun et al., 2012). To focus the relatively smaller cells found in blood, such as white blood cells (WBCs), a microfluidic device must contain curves with a high curvature ratio.

Hence, besides the focusing of particles, it is also crucial to have the proper curvature for sized separation (Figure S1). In the situation of high curvature ratio, where F_D dominates, particles could be dispersed and lose their focusing due to the insufficiency of F_z, or all the particles with different sizes could be pushed to the same focusing position due to the strong migration force (F_D) (Martel and Toner, 2013). In a curve with extremely low curvature ratio, where F_z dominates, particles with different sizes remain at the same equilibrium positions similar to a straight channel due to the limited migration force (Martel and Toner, 2013). Since the inertial lift is proportional to the fourth power of the diameter of the particles, stronger mixing forces are required to move the smaller particles to equilibrium positions in order to achieve better focusing of these particles; consequently, the conventional spiral devices are less successful in focusing smaller WBCs, resulting in low purities. An accurate design of curves in the microfluidic structure would lead to the focusing of cells while separating CTCs and blood cells by size. To address the challenge of focusing of smaller cells, such as WBCs, we designed Labyrinth incorporating extra geometrical features. The major difference between Labyrinth and all other spiral designs is the numerous sharp corners placed across the flow pattern. These corners have sharper curvatures compared with the milder curvatures of the "loops" in typical spiral channels, and hence enhance Dean forces to migrate particles toward their equilibrium positions. The combination of long loops and sharp corners results in clean but separated focusing of both large (CTCs) and small (WBCs) cells, while most spiral devices have to compromise for either low CTC recovery or low WBC removal as the smaller cells are not efficiently focused.

Labyrinth Specifications

The total channel length of Labyrinth is 637 mm. It is 500 μm in width and 100 μm in height. It consists of 11 loops and 56 corners. The loops (Figure 1B), which have a small curvature ratio (δ) (Equation 4), range from 5.29×10^{-3} m^{-1} to 3.70×10^{-2} m^{-1}, and were incorporated into Labyrinth to provide enough length of channel to achieve total focusing of cells and to have the proper curvature for the separation between CTCs and blood cells. The 56 sharp right-angle corners (Figure 1C), which have high curvature ratio, further enhance the focusing of smaller cells without the need for positive or negative selection. The channel

width expands to 1,000 μm from 500 μm before the streams are diverted into the outlets (Figure 1D). The outlets were designed such that the focused individual streams could be collected separately (Figures 1E and S1).

Cell Focusing in Labyrinth

To demonstrate cell focusing in Labyrinth, DAPI-labeled WBCs with GFP-labeled breast cancer cells (MCF-7) were mixed in PBS buffer and flowed through Labyrinth. Figure 1F presents a fluorescent image (green, MCF-7 GFP; blue, WBCs) of the entire device. The corners in the device are numbered in sequential order from inlet to outlet. Cancer cells in Labyrinth started focusing at corner no. 5 (50 mm from inlet), whereas WBCs became focused at corner no. 47 (480 mm from inlet), as shown in Figure 1F. The difference in the length needed for the cells to be focused resulted from the magnitude of lift force, which was proportional to the fourth power of particle size (Equation 1). Given that the smaller cells encounter lower lift forces compared with big cells, it is harder to focus the smaller cells in inertial fluidics devices. Smaller cells require longer time to come to the equilibrium positions as the force experienced by them is much smaller compared with bigger cells (Figure S1). Hence the smaller cells need longer travel distance to be able to focus fully. In addition, Labyrinth design incorporated multiple turns to aid the focusing of smaller cells further (Figure S1). Focused WBCs were sorted out into the first outlet and the CTCs stream was collected through the second outlet as shown in Figure 1E.

Testing and Optimization of Labyrinth for Cell Recovery

Labyrinth was optimized and tested for inertial separation of cancer cells using human breast (MCF-7), pancreatic (PANC-1), prostate (PC-3), and lung (H1650) cancer cell lines. It was determined that the optimal flow rate for maximized recovery and purity was 2.5 mL/min (Figure S2), and also that it takes 60 s for the flow to stabilize in the device for optimal collection (Figure S2). Pre-labeled (Cell Tracker) cancer cells and WBCs were spiked at a high concentration (~100,000/mL and ~500,000/mL, respectively) into buffer and separated using Labyrinth. Using MCF-7 cells, 91.5% ± 0.9% of cancer cells were recovered from the second outlet, while 91.4% ± 3.3% of WBCs were removed through the first outlet (Figure 2A). With GFP-labeled PANC-1 cells, a similar separation was achieved, with 92.4% ± 3.2% recovery of cancer cells and 89.0% ± 1.1% of WBCs removed in the first outlet (Figure 2A). Labyrinth recovery was further tested with other solid tumor cell types, such as lung and prostate, and found the yields to be similar (Figure 2A). MCF-7 and PC-3 cells were spiked into whole blood and run through Labyrinth without any pre-processing. The recoveries even from whole blood are higher than 90% (Figure 2A). Separation of cancer cells from other blood cells was visualized using a high-speed camera and, as shown in Figure 2B, the cell streams were physically separate. To further characterize the ability of Labyrinth to isolate lower concentrations of CTCs (100/mL), MCF-7/GFP cells were spiked into buffer and into healthy donor blood samples, and then processed through Labyrinth. In this set of experiments, blood is treated with Dextran following the spike to remove excess red blood cells (RBCs) and see its effect on recovery. The average recovery in buffer solution was 94.4% ± 3.8%, while in RBC-depleted blood a 95.3% ± 0.7% recovery was obtained (Figure 2C). Importantly, an MTT assay demonstrated that the shear stress experienced by cells processed through Labyrinth did not affect the cell viability or the proliferation ability (Figures 2D and 2E).

Double Labyrinth Separation for Higher Specificity

Processing of samples through a single Labyrinth, even at a flow rate of 2.5 mL/min, which is considerably greater than the currently available label-free techniques, yielded comparable or better purity (13,800 WBCs/mL average, n = 9, compared with 32,000 WBCs/mL reported [Ozkumur et al., 2013]). However, to further increase CTC enrichment for high-content downstream molecular assays at single-cell resolution we adopted the strategy of using a double Labyrinth, two single Labyrinth devices applied in series. This system further reduces the WBC contamination yet maintains equivalent CTC viability. As shown in Figures 2F and 2G, the recovery of MCF-7 cells using a double Labyrinth (91.1% ± 0.7%) was consistent with the results obtained using a single Labyrinth (91.5% ± 0.9%), but with lower WBC contamination (663 ± 647 WBCs/mL), representing a two-log improvement in tumor cell enrichment over the single Labyrinth. This mode of operation yields higher purity than reported using other label-free methods (Ding et al., 2014; Hyun et al., 2013; Khoja et al., 2012; Kim et al., 2014; Li et al., 2015; Liu et al., 2013; Ozkumur et al., 2013; Pailler et al., 2013; Russom et al., 2009; Sun et al., 2012; Vona et al., 2004). It is to be noted that the additional run through Labyrinth adds less than 5 min to the total time versus a single run.

Isolation of CTCs from Pancreatic Cancer Patients

CTC analysis was performed using blood samples collected from 20 patients with a new diagnosis of pancreatic cancer, as shown in Figure 3A. These whole-blood samples were all processed without any pre-processing (as described in the STAR Methods). All of the samples had measurable CTCs, identified as DAPI-positive nucleated cells staining positive for CK-19 and negative for CD45. CTC enumeration in these 20 patients showed a yield of 51.6 ± 25.5 pancreatic CTCs/mL blood, whereas less than 2 CTC-like cells/mL were found in healthy controls. Patient demographics are provided in Table S1.

Pancreatic CTCs were further evaluated to determine what percentage of the cells displayed epithelial versus mesenchymal-like features. To quantitate epithelial-like cells, expression of EpCAM and CK-19 was assessed, while for quantification of mesenchymal-like cells, the EMT markers ZEB1 and ATDC were used. All patient samples contained not only CK+ CTCs but also EMT marker-positive CTCs. An average of 53% ± 17% of the captured CTCs stained positive for EMT-related markers along with CK-19. Figure 3B presents three CTC subpopulations obtained from the same patient differentially expressing epithelial and mesenchymal markers, demonstrating intra-patient CTC heterogeneity. The molecular characteristics of CTCs were further explored by mutational analysis of select genes using the DNA isolated from captured CTCs. DNA was extracted from CTCs isolated from five pancreatic patient samples. The qBiomarker Somatic Mutation PCR Array: Human Pancreatic Cancer (QIAGEN) was chosen to represent a comprehensive spectrum of frequently mutated genes in pancreatic cancer. The array includes multiple assays for genes including APC, BRAF, CDKN2A, CTNNB1, KRAS, NRAS, PIK3CA, SMAD4, and TP53.

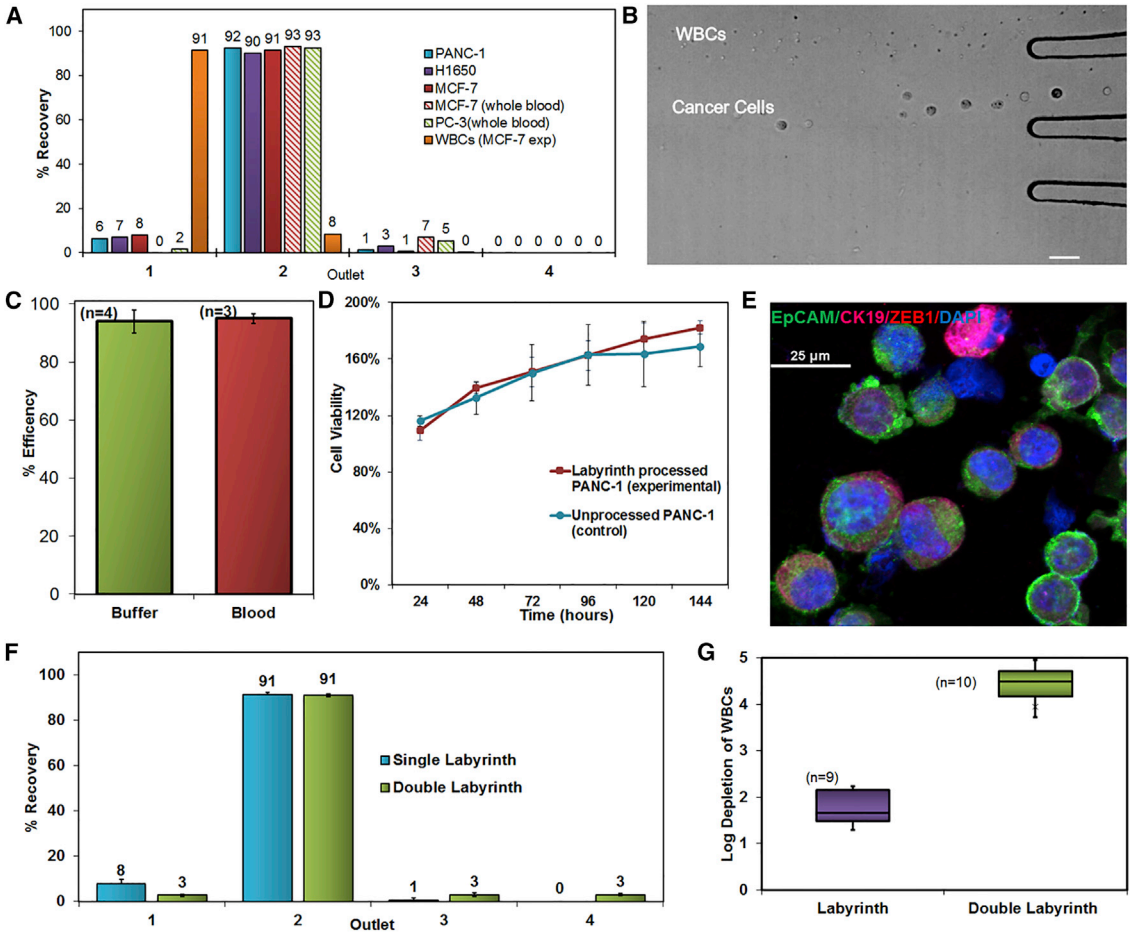

Figure 2. Control Experiments with Spiked Cancer Cell Lines Using Labyrinth

(A) Recovery results from each outlet of Labyrinth for four different cancer cell lines: breast (MCF-7), pancreatic (PANC-1), prostate (PC-3), and lung (H1650) cancer, along with white blood cells (WBCs). PANC-1 (n = 3), H1650 (n = 1), and MCF-7 (n = 3) were spiked into RBC-removed blood, whereas MCF-7 (n = 3) and PC-3 (n = 1) were spiked into whole blood.

(B) High-speed camera image showing Labyrinth's ability to separate WBCs from cancer cells through first and second outlet. Scale bar, 100 μm.

(C) Recovery results from second outlet using 100 MCF-7 cells for both buffer experiments (n = 4) and spiked cells in whole blood (n = 3).

(D) MTT assay results for Labyrinth-processed PANC-1 cells (n = 8) and cultured over a period of 7 days.

(E) Fluorescence image showing morphology preservation of PANC-1 cells processed at 2.5 mL/min.

(F) Comparison of recovery efficiency using a single or double Labyrinth for each outlet. Error bars represent the SD of three replicates.

(G) Log depletion of WBCs using the single (n = 9) and double Labyrinth (n = 10) to demonstrate high device purity.

Using this array, mutations in at least one gene were detected in all samples tested (Figure S3). All of the samples tested were positive for mutations in KRAS, which is mutated in not only PDAC patients (>95%), but also in pancreatic intraepithelial neoplasias, the earliest pre-neoplastic stages of pancreatic cancer progression (Kanda et al., 2012). As expected, no mutations were detected in the healthy control.

Isolation of CTCs from Breast Cancer Patients

Blood samples were treated with Dextran (as described in the STAR Methods) prior to running through Labyrinth to prevent RBC interference with single-cell analysis. However, in a small cohort of breast cancer patients, whole-blood samples were run similar to pancreatic cancer samples and CTCs were successfully isolated (Figure S3). A total of 56 blood samples obtained from patients with metastatic breast cancer were processed through Labyrinth to isolate CTCs. Of these, nine samples were processed using a single Labyrinth approach. As shown in Figure 3C, the average number of CTCs recovered from the breast cancer patients was 9.1 CTCs/mL (range 3–31). We processed the rest of the samples using the strategy of double Labyrinth. In three patients, we did side-by-side comparison of single and double Labyrinth analysis and found that although the CTCs yields were comparable (Figure S3), the double Labyrinth processing reduced WBC contamination by two orders of magnitude more than the single Labyrinth. In the 40 patient samples processed using the double Labyrinth strategy, the recovery of CTCs was 5.4 ± 4.6 CTCs/mL (range 0–21.7; Figure 3D). Figure 3E presents the number of WBCs in the enriched CTC population (663 ± 647 WBCs/mL, range 0–2,900), which is by far the best purity reported among label-free methods. CTCs were identified as DAPI-positive nucleated cells

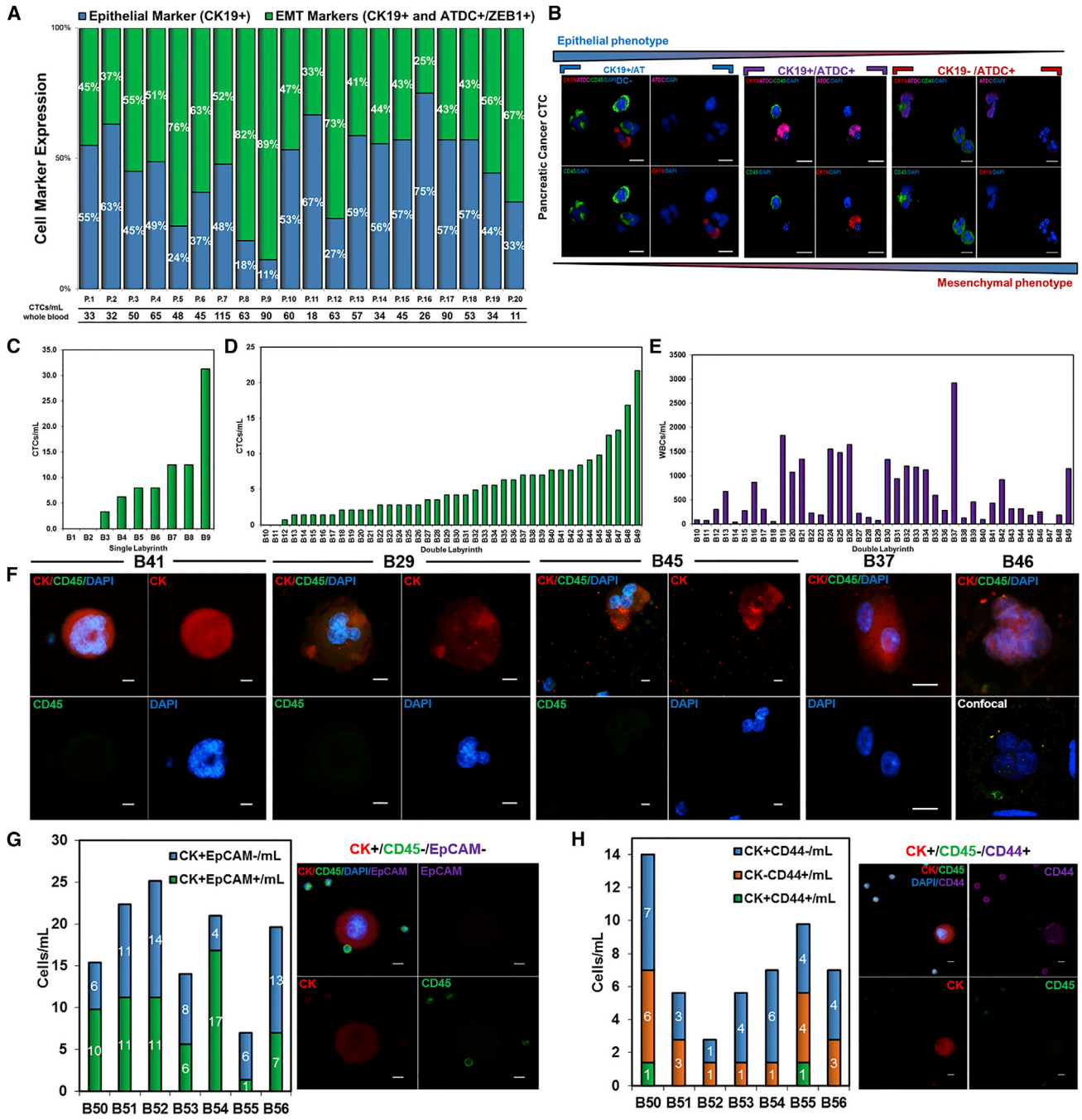

Figure 3. Results of Pancreatic and Breast Cancer Patient Samples Using Labyrinth

(A) Percentage of CTCs expressing both EMT and epithelial markers versus only epithelial markers. Column on the bottom indicates the total CTCs (CK+, CD45−, DAPI+) per mL of blood for each patient.

(B) Immunocytochemistry analysis performed on a metastatic sample where both epithelial and EMT-like CTC subpopulations were found. Scale bars, 10 μm.

(C) CTCs (CK+, CD45−, DAPI+) per mL for each patient sample processed with single Labyrinth.

(D) CTCs per mL for each patient sample processed with double Labyrinth.

(E) WBCs per mL for each patient sample processed with double Labyrinth.

(F) Fluorescence microscopy images demonstrating typical, multi-nuclei, and clusters of CTCs separated by Labyrinth. Cells are stained with DAPI (blue), cytokeratin (red), and CD45 (green).

(G) Representative images of CTCs with or without the expression of cytokeratin and EpCAM.

(H) Number of CTCs with or without the expression of cytokeratin and CD44. Scale bars, 10 μm.

that stained positive for pan-CK and negative for CD45. Figure 3F (along with Figure S3) illustrates typical CTCs recovered from the double Labyrinth (B41), including multi-nucleated CTC (B29), and clusters of CTCs (B45, B37, and B46). Since the clusters are of larger size, they preferably migrate to the second outlet, which is the target collection outlet for CTCs.

In addition, enriched CTCs from Labyrinth were stained using antibodies against the epithelial marker EpCAM and the CSC and EMT marker CD44. The results are presented in Figures 3G and 3H. In all seven of the patients who were analyzed, we found CTCs that did not express EpCAM (Figure 3G). These cells would not have been identified as CTCs in EpCAM-based, affinity-based capture techniques. Indeed, 52.3% ± 19.5% of the CK+ CTCs were EpCAM− and 47.7% ± 19.5% were EpCAM+. None of the isolated cells was observed to be EpCAM+/CK−. For the same seven patients, we found CTCs that express CD44 in all of the patients (Figure 3H). Among these samples, 41.7% ± 14.1% of the CTCs were CD44+ and 58.3% ± 14.1% were CD44−. Cells expressing CD44+/CK− were only observed in two of the patients. Hence, Labyrinth is capable of both isolating heterogeneous single CTCs and clusters of CTCs.

Single-Cell Multiplex Gene Expression Analysis of CTCs

We previously utilized molecular profiling to characterize the gene expression patterns of EMT and MET CSCs from a series of primary human breast cancers (Liu et al., 2014). Utilizing these data, we identified a 96 gene signature whose expression characterized and discriminated these differing CSC populations (Table S3). Among these genes are the epithelial CSC marker ALDH1a3 and the mesenchymal CSC marker CD44, as well as other genes involved in "stemness" and/or EMT/MET transitions. We utilized multiplex qRT-PCR to interrogate expression of each of these 96 genes in single CTCs isolated using double Labyrinth purification followed by C1 and BioMark HD (Fluidigm, USA) analysis. We found that the MCF-7 cells (which are of luminal phenotype) exhibit high expression of E-Cadherin, PROM1, EpCAM, ERBB2, and ALDH1a3, whereas the Basal/Claudin^{Low} phenotype SUM159 cells expressed N-Cadherin, Zeb-1, Vimentin, TGF-β1, and CD44. Accordingly, and based on our previous work (Liu et al., 2014), we classified the cells with the former signature as MET and the later signature as EMT. Based on these gene expression patterns, we classified CTCs into four different groups: CK CTCs, EMT CTCs, MET CTCs, and Dual (EMT-MET) CTCs (Table S4).

Figure S4 depicts the heatmap of the gene expression analysis of 47 single cells, including 31 patient-derived CTCs from 6 different patients, 8 patient-derived contaminating WBCs (Pts-WBCs), and 8 WBCs from healthy controls (HC-WBCs). The genes are grouped together based on the genotypic characterization including, but not limited to, epithelial, mesenchymal, oncogenic, and blood-related genes. CTCs presented a gene expression pattern that was distinct from WBCs, whereas Pts-WBCs were similar to HC-WBCs. However, the CTCs had varied profiles of gene expression. Patient A CTC exhibited MET profile, whereas patient B had two CK CTCs and one EMT CTC. Patients C and D had several Dual CTCs along with CK CTCs. On the other hand, patient E had several CTCs, all of which were CK CTCs. Patient F had a total of 16 CTCs that were analyzed on the Fluidigm BioMark HD chip, of which 6 were MET CTCs, 6 were CK CTCs, and 4 were EMT CTCs. Figure 4 presents the examples of inter- and intra-patient heterogeneity of CTCs along with relative expression levels of the relevant genes shown in a Violin plot for HC-WBCs (n = 8), Pt-WBCs (n = 8), CK CTCs from two different patients B and C (n = 2 each), along with EMT and MET CTCs. As shown in Figure 4A, the sample from patient A was found to have a MET CTC characterized by CDH1+/EpCAM+/ALDH1a3+/PTPRC−, whereas the sample from patient B presents an EMT CTC characterized by CDH2+/EpCAM−/CD44+/CD24−/ PTPRC−. Samples from patients B and C contained CTCs that did not express CSC markers, but were CK+/ PTPRC−. Overall, MET CTCs expressed EpCAM, ALDH1a3, and CDH1 (E-Cadherin), and low levels of Vimentin, whereas EMT CTCs expressed Vimentin, CD44, and CDH2 (N-Cadherin), and low levels of ALDH1a3 and CD24. A detailed characterization of all the different categories is presented in Table S4. Furthermore, principal-component analysis (PCA) showed separation of CTCs from the contaminating blood cells (Figure 4B). In control experiments with technical and biological replicates using the T47D breast cancer cell line, the expression profiles variation was found to be minimal, indicating that the variation of profiles among single cells is reliable and reproducible. The single-cell gene expression analysis of 16 CTCs isolated from a single breast cancer patient (patient F), whose primary tumor was ER+/PR+/HER2− showed three distinct groups of CTCs in the unsupervised cluster analysis including: EMT CTCs (n = 4) characterized by CD44+/CD24−/Vimentin+/ALDH1a3−/PTPRC−, MET CTCs (n = 6) characterized by ALDH1a3+/SOCS3+/Twist1+/CD24+/CD44−/Vimentin−/PTPRC−, and CK CTCs (n = 6) characterized by KRT18+/KRT19+/PTPRC−. The Log2 expression values for genes in each of these subpopulations are presented as a Violin plot in Figure 4C. In addition, the expression profiles of three groups of CTCs were distinctly different from each other, as clearly demonstrated by the PCA analysis (Figure 4D).

DISCUSSION

Although application of microfluidics to cancer research is nascent, a number of studies have demonstrated its feasibility in the isolation and characterization of CTCs from clinical samples (Nagrath et al., 2007; Ozkumur et al., 2013; Peeters et al., 2013). To sort the WBCs from CTCs in a truly label-free fashion we developed a strategy using inertial microfluidics, which not only uses the delicate balance of inertial and Dean forces to differentially focus cells, but also induces fluidic path directional shift by incorporating 56 high curvature turns. Unlike other inertial focusing methods, the multi-course path traversing across inner loops to outer loops yields highest hydrodynamic path length (637mm) to enhance the focusing of both CTCs and WBCs resulting highest purity.

With the recent advances in tools for genomic characterization, it is more compelling than ever to look at the tumor heterogeneity to understand tumor progression and resistance to therapies. The Labyrinth device enabled high yields of CTCs without the bias induced by antibody-based selection, allowing the identification of true biological tumor heterogeneity. Twenty milliliters of blood was processed in less than 30 min to obtain live tumor cell suspension, which, upon single-cell characterization,

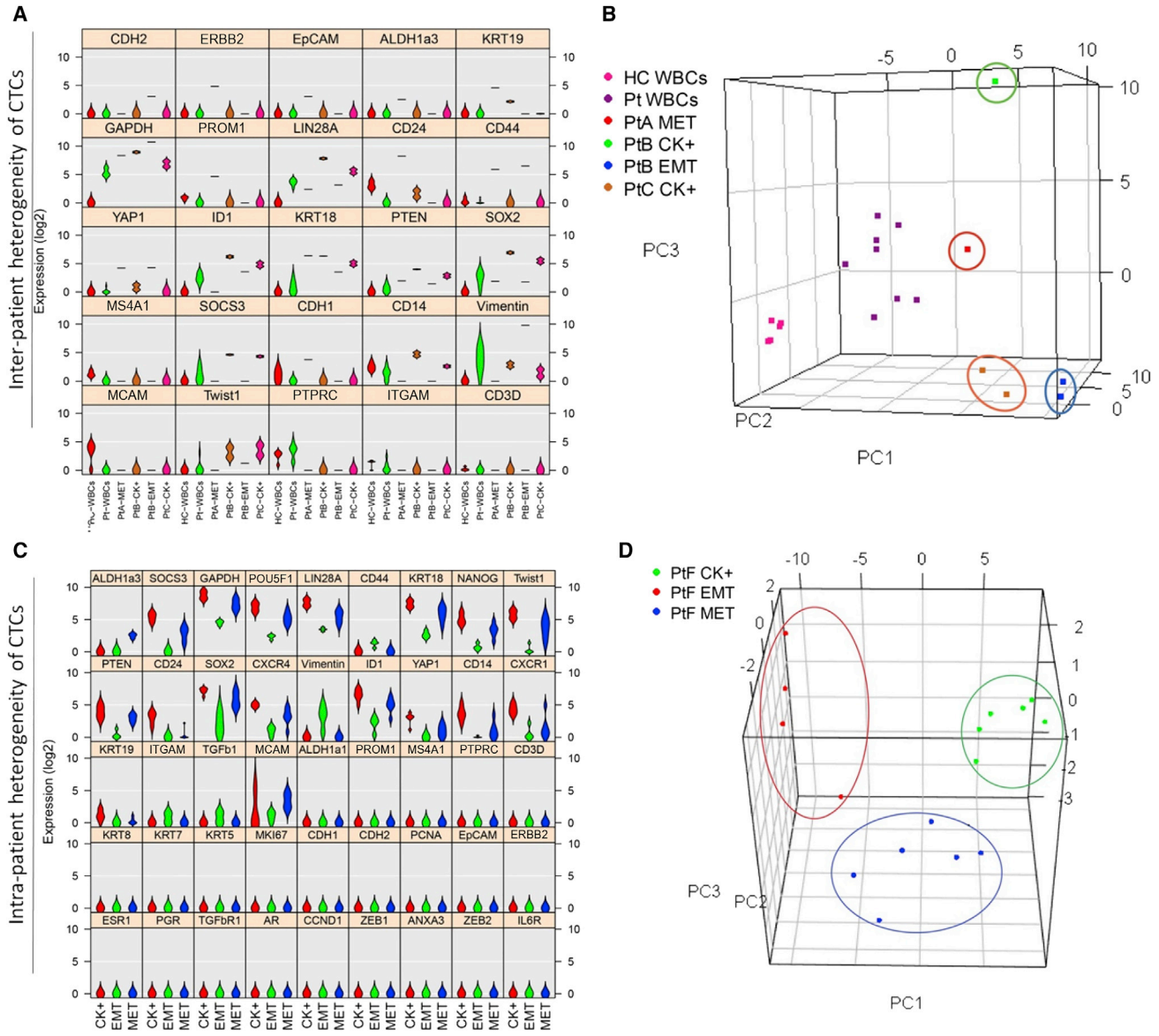

Figure 4. Inter- and Intra-patient Heterogeneity of Patient-Derived CTCs

(A and B) Violin plot of Log2 expression of genes (A) and PCA (B) show the inter-patient heterogeneity between healthy controls (HC-WBCs), patient-derived contaminating WBCs (Pt-WBCs), and patient-derived CTCs from patients A, B, and C.

(C and D) The Log2 gene expression data are also presented for 16 single CTCs isolated from a single breast cancer patient (PtF) in Violin plot (C) and PCA (D). These 16 single CTCs show intra-patient heterogeneity as three distinct signatures are observed: MET (ALDH+) and EMT (CD44+/CD24−) CSCs, and CK+ non-CSCs.

pointed to distinct subpopulations of tumor stem cells in circulation. The key genomic signatures from our studies can be further validated in future studies involving large cohorts of patients along with profiling matching tissues whenever possible. In addition, our approach can be readily applied in future clinical studies by incorporating single-cell genomic profiling of CTCs isolated from the Labyrinth as biomarkers of response/resistance to monitor targeted therapies in breast and other solid tumors. Although we have incorporated Fluidigm technology for the downstream analysis, Labyrinth output can be used with other downstream single-cell tools including, but not limited to, DEPArray (by Silicon Biosystems) and droplet digital PCR (Raindance) (Bingham et al., 2017; Perkins et al., 2017). Future research will involve more extensive application of innovative microfluidic systems that target the use of CTCs for early detection, treatment selection, and monitoring of cancer patients.

STAR★METHODS

Detailed methods are provided in the online version of this paper and include the following:

- KEY RESOURCES TABLE
- CONTACT FOR REAGENT AND RESOURCE SHARING

SUPPLEMENTAL INFORMATION

Supplemental Information includes four figures, four tables, and one movie and can be found with this article online at http://dx.doi.org/10.1016/j.cels.2017.08.012.

AUTHOR CONTRIBUTIONS

E.L., L.R., and S.F. contributed equally and wrote the manuscript. E.L., H.Y., and S.N. designed the device. E.A. and M.W. designed and supervised single-cell molecular profiling. E.L., S.F., L.R., H.Y., L.R., Y.D., L.W., and E.A. performed experiments and analyzed data. V.S, D.S., M.B., and M.W. supervised the clinical samples. All authors discussed the results and commented on the manuscript. M.S.W. has financial holdings and is a scientific advisor for OncoMed Pharmaceuticals, is a scientific advisor for Verastem, Paganini, and MedImmune, and receives research support from Dompe Pharmaceuticals, MedImmune, Paganini, and Cormorant Pharmaceuticals.

ACKNOWLEDGMENTS

This work was supported by the NIH Director's New Innovator Award (1DP2OD006672-01), a Career Development Program of the Gastrointestinal Specialized Program of Research Excellence (GI SPORE) award (CA 130810), Shared Instrumentation Grant (SIG) Program (S10OD16187), Cancer Center Support Grant (P30 CA046592), and a Department of Defense (DoD) Office of the Congressionally Directed Medical Research Programs (CDMRP) Career Development Award to S.N. This work received additional support from grants from NIH (2R01CA129765-06A1), BCRF, and MedImmune awarded to M.S.W. Clinical sample collection was supported by Fashion Footwear Charitable Foundation of New York/QVC Presents Shoes on Sale.

Received: December 13, 2016
Revised: April 24, 2017
Accepted: August 22, 2017
Published: September 20, 2017

REFERENCES

ASMOLOV, E.S. (1999). The inertial lift on a spherical particle in a plane Poiseuille flow at large channel Reynolds number. J. Fluid Mech. *381*, 63–87.

Bednarz-Knoll, N., Alix-Panabieres, C., and Pantel, K. (2012). Plasticity of disseminating cancer cells in patients with epithelial malignancies. Cancer Metastasis Rev. *31*, 673–687.

Bingham, C., Fernandez, S.V., Fittipaldi, P., Dempsey, P.W., Ruth, K.J., Cristofanilli, M., and Katherine Alpaugh, R. (2017). Mutational studies on single circulating tumor cells isolated from the blood of inflammatory breast cancer patients. Breast Cancer Res. Treat. *163*, 219–230, 1–12.

Brooks, M.D., Burness, M.L., and Wicha, M.S. (2015). Therapeutic implications of cellular heterogeneity and plasticity in breast cancer. Cell Stem Cell *17*, 260–271.

Di Carlo, D., Irimia, D., Tompkins, R.G., and Toner, M. (2007). Continuous inertial focusing, ordering, and separation of particles in microchannels. Proc. Natl. Acad. Sci. USA *104*, 18892–18897.

Dawson, S.J., Tsui, D.W., Murtaza, M., Biggs, H., Rueda, O.M., Chin, S.F., Dunning, M.J., Gale, D., Forshew, T., Mahler-Araujo, B., et al. (2013). Analysis of circulating tumor DNA to monitor metastatic breast cancer. N. Engl. J. Med. *368*, 1199–1209.

Ding, X., Peng, Z., Lin, S.C., Geri, M., Li, S., Li, P., Chen, Y., Dao, M., Suresh, S., and Huang, T.J. (2014). Cell separation using tilted-angle standing surface acoustic waves. Proc. Natl. Acad. Sci. USA *111*, 12992–12997.

Gossett, D.R., and Carlo, D.D. (2009). Particle focusing mechanisms in curving confined flows. Anal. Chem. *81*, 8459–8465.

Hyun, K.-A., Kwon, K., Han, H., Kim, S.-I., and Jung, H.-I. (2013). Microfluidic flow fractionation device for label-free isolation of circulating tumor cells (CTCs) from breast cancer patients. Biosens. Bioelectron. *40*, 206–212.

Jackson, J.M., Witek, M.A., Kamande, J.W., and Soper, S.A. (2017). Materials and microfluidics: enabling the efficient isolation and analysis of circulating tumour cells. Chem. Soc. Rev. *46*, 4245–4280.

Kanda, M., Matthaei, H., Wu, J., Hong, S.M., Yu, J., Borges, M., Hruban, R.H., Maitra, A., Kinzler, K., Vogelstein, B., et al. (2012). Presence of somatic mutations in most early-stage pancreatic intraepithelial neoplasia. Gastroenterology *142*, 730–733.e739.

Karabacak, N.M., Spuhler, P.S., Fachin, F., Lim, E.J., Pai, V., Ozkumur, E., Martel, J.M., Kojic, N., Smith, K., and Chen, P.-i. (2014). Microfluidic, marker-free isolation of circulating tumor cells from blood samples. Nat. Protoc. *9*, 694–710.

Khoja, L., Backen, A., Sloane, R., Menasce, L., Ryder, D., Krebs, M., Board, R., Clack, G., Hughes, A., Blackhall, F., et al. (2012). A pilot study to explore circulating tumour cells in pancreatic cancer as a novel biomarker. Br. J. Cancer *106*, 508–516.

Kim, T.H., Yoon, H.J., Stella, P., and Nagrath, S. (2014). Cascaded spiral microfluidic device for deterministic and high purity continuous separation of circulating tumor cells. Biomicrofluidics *8*, 064117.

Krebs, M.G., Metcalf, R.L., Carter, L., Brady, G., Blackhall, F.H., and Dive, C. (2014). Molecular analysis of circulating tumour cells-biology and biomarkers. Nat. Rev. Clin. Oncol. *11*, 129–144.

Labib, M., Green, B., Mohamadi, R.M., Mepham, A., Ahmed, S.U., Mahmoudian, L., Chang, I.H., Sargent, E.H., and Kelley, S.O. (2016). Aptamer and antisense-mediated two-dimensional isolation of specific cancer cell subpopulations. J. Am. Chem. Soc. *138*, 2476–2479.

Li, P., Mao, Z., Peng, Z., Zhou, L., Chen, Y., Huang, P.-H., Truica, C.I., Drabick, J.J., El-Deiry, W.S., Dao, M., et al. (2015). Acoustic separation of circulating tumor cells. Proc. Natl. Acad. Sci. USA *112*, 4970–4975.

Lin, H.K., Zheng, S., Williams, A.J., Balic, M., Groshen, S., Scher, H.I., Fleisher, M., Stadler, W., Datar, R.H., Tai, Y.C., et al. (2010). Portable filter-based microdevice for detection and characterization of circulating tumor cells. Clin. Cancer Res. *16*, 5011–5018.

Liu, Z., Huang, F., Du, J., Shu, W., Feng, H., Xu, X., and Chen, Y. (2013). Rapid isolation of cancer cells using microfluidic deterministic lateral displacement structure. Biomicrofluidics *7*, 11801.

Liu, S., Cong, Y., Wang, D., Sun, Y., Deng, L., Liu, Y., Martin-Trevino, R., Shang, L., McDermott, S.P., Landis, M.D., et al. (2014). Breast cancer stem cells transition between epithelial and mesenchymal states reflective of their normal counterparts. Stem Cell Rep. *2*, 78–91.

Luo, M., Brooks, M., and Wicha, M.S. (2015). Epithelial-mesenchymal plasticity of breast cancer stem cells: implications for metastasis and therapeutic resistance. Curr. Pharm. Des. *21*, 1301–1310.

Maheswaran, S., Sequist, L.V., Nagrath, S., Ulkus, L., Brannigan, B., Collura, C.V., Inserra, E., Diederichs, S., Iafrate, A.J., Bell, D.W., et al. (2008). Detection of mutations in EGFR in circulating lung-cancer cells. N. Engl. J. Med. *359*, 366–377.

Martel, J.M., and Toner, M. (2013). Particle focusing in curved microfluidic channels. Sci. Rep. *3*.

Nagrath, S., Sequist, L.V., Maheswaran, S., Bell, D.W., Irimia, D., Ulkus, L., Smith, M.R., Kwak, E.L., Digumarthy, S., Muzikansky, A., et al. (2007). Isolation of rare circulating tumour cells in cancer patients by microchip technology. Nature *450*, 1235–1239.

Ozkumur, E., Shah, A.M., Ciciliano, J.C., Emmink, B.L., Miyamoto, D.T., Brachtel, E., Yu, M., Chen, P.-i., Morgan, B., Trautwein, J., et al. (2013). Inertial focusing for tumor antigen-dependent and -independent sorting of rare circulating tumor cells. Sci. Transl. Med. *5*, 179ra147.

Pailler, E., Adam, J., Barthelemy, A., Oulhen, M., Auger, N., Valent, A., Borget, I., Planchard, D., Taylor, M., Andre, F., et al. (2013). Detection of circulating tumor cells harboring a unique ALK rearrangement in ALK-positive non-small-cell lung cancer. J. Clin. Oncol. *31*, 2273–2281.

Pantel, K., and Speicher, M.R. (2016). The biology of circulating tumor cells. Oncogene *35*, 1216–1224.

Paterlini-Brechot, P., and Benali, N.L. (2007). Circulating tumor cells (CTC) detection: clinical impact and future directions. Cancer Lett. *253*, 180–204.

Peeters, D.J., De Laere, B., Van den Eynden, G.G., Van Laere, S.J., Rothe, F., Ignatiadis, M., Sieuwerts, A.M., Lambrechts, D., Rutten, A., van Dam, P.A., et al. (2013). Semiautomated isolation and molecular characterisation of single or highly purified tumour cells from CellSearch enriched blood samples using dielectrophoretic cell sorting. Br. J. Cancer *108*, 1358–1367.

Perkins, G., Lu, H., Garlan, F., and Taly, V. (2017). Chapter three - droplet-based digital PCR: application in cancer research. In Advances in Clinical Chemistry, S.M. Gregory, ed. (Elsevier), pp. 43–91.

Reya, T., Morrison, S.J., Clarke, M.F., and Weissman, I.L. (2001). Stem cells, cancer, and cancer stem cells. Nature *414*, 105–111.

Russom, A., Gupta, A.K., Nagrath, S., Di Carlo, D., Edd, J.F., and Toner, M. (2009). Differential inertial focusing of particles in curved low-aspect-ratio microchannels. New J. Phys. *11*, 75025.

Segré, G., and Silberberg, A. (1961). Radial particle displacements in Poiseuille flow of suspensions. Nature *189*, 209–210.

Sehl, M.E., Shimada, M., Landeros, A., Lange, K., and Wicha, M.S. (2015). Modeling of cancer stem cell state transitions predicts therapeutic response. PLoS One *10*, e0135797.

Sheng, W., Ogunwobi, O.O., Chen, T., Zhang, J., George, T.J., Liu, C., and Fan, Z.H. (2014). Capture, release and culture of circulating tumor cells from pancreatic cancer patients using an enhanced mixing chip. Lab. Chip *14*, 89–98.

Silberberg, G.S.a.A. (1962). Behaviour of macroscopic rigid spheres in Poiseuille flow. J. Fluid Mech. *14*, 22.

Speicher, M.R. (2013). Single-cell analysis: toward the clinic. Genome Med. *5*, 74.

Stott, S.L., Hsu, C.H., Tsukrov, D.I., Yu, M., Miyamoto, D.T., Waltman, B.A., Rothenberg, S.M., Shah, A.M., Smas, M.E., Korir, G.K., et al. (2010a). Isolation of circulating tumor cells using a microvortex-generating herringbone-chip. Proc. Natl. Acad. Sci. USA *107*, 18392–18397.

Stott, S.L., Lee, R.J., Nagrath, S., Yu, M., Miyamoto, D.T., Ulkus, L., Inserra, E.J., Ulman, M., Springer, S., Nakamura, Z., et al. (2010b). Isolation and characterization of circulating tumor cells from patients with localized and metastatic prostate cancer. Sci. Transl. Med. *2*, 25ra23.

Sun, J., Li, M., Liu, C., Zhang, Y., Liu, D., Liu, W., Hu, G., and Jiang, X. (2012). Double spiral microchannel for label-free tumor cell separation and enrichment. Lab. Chip *12*, 3952–3960.

Vona, G., Estepa, L., Beroud, C., Damotte, D., Capron, F., Nalpas, B., Mineur, A., Franco, D., Lacour, B., Pol, S., et al. (2004). Impact of cytomorphological detection of circulating tumor cells in patients with liver cancer. Hepatology *39*, 792–797.

Yoon, H.J., Shanker, A., Wang, Y., Kozminsky, M., Jin, Q., Palanisamy, N., Burness, M.L., Azizi, E., Simeone, D.M., Wicha, M.S., et al. (2016). Tunable thermal-sensitive polymer-graphene oxide composite for efficient capture and release of viable circulating tumor cells. Adv. Mater. *28*, 4891–4897.

Yu, M., Ting, D.T., Stott, S.L., Wittner, B.S., Ozsolak, F., Paul, S., Ciciliano, J.C., Smas, M.E., Winokur, D., Gilman, A.J., et al. (2012). RNA sequencing of pancreatic circulating tumour cells implicates WNT signalling in metastasis. Nature *487*, 510–513.

Yu, M., Bardia, A., Wittner, B., Stott, S.L., Smas, M.E., Ting, D.T., Isakoff, S.J., Ciciliano, J.C., Wells, M.N., Shah, A.M., et al. (2013a). Circulating breast tumor cells exhibit dynamic changes in epithelial and mesenchymal composition. Science *339*, 580–584.

Yu, X., He, R., Li, S., Cai, B., Zhao, L., Liao, L., Liu, W., Zeng, Q., Wang, H., Guo, S.S., et al. (2013b). Magneto-controllable capture and release of cancer cells by using a micropillar device decorated with graphite oxide-coated magnetic nanoparticles. Small *9*, 3895–3901.

Zhang, L., Ridgway, L.D., Wetzel, M.D., Ngo, J., Yin, W., Kumar, D., Goodman, J.C., Groves, M.D., and Marchetti, D. (2013). The identification and characterization of breast cancer CTCs competent for brain metastasis. Sci. Transl. Med. *5*, 180ra148.

STAR★METHODS

KEY RESOURCES TABLE

REAGENT or RESOURCE	SOURCE	IDENTIFIER
Antibodies		
Mouse Anti-Cytokeratin (clone CAM 5.2)	BD Biosciences	Cat# 349205; RRID: AB_2134314
Mouse Anti-Human CD45 (clone HI30)	BD Biosciences	Cat# 555480; RRID: AB_395872
Rabbit Anti-ZEB1	Bethyl Lab	Cat# A301-921A; RRID: AB_1524109
Donkey Anti-Rat IgG (H+L) Secondary Antibody, Alexa Fluor 488	Thermo Fisher	Cat# A21208; RRID: AB_141709
Donkey Anti-Rabbit IgG (H+L) Secondary Antibody, Alexa Fluor 568	Thermo Fisher	Cat# A10042; RRID: AB_2534017
Donkey Anti-Mouse IgG (H+L) Secondary Antibody, Alexa Fluor 647	Thermo Fisher	Cat# A31571; RRID: AB_162542
Goat Anti-Mouse IgG1 Secondary Antibody, Alexa Fluor 488	Thermo Fisher	Cat# A21121; RRID: AB_141514
Goat anti-Rabbit IgG (H+L) Secondary Antibody, Alexa Fluor 546	Thermo Fisher	Cat# A11035; RRID: AB_143051
Avidin, NeutrAvidin, Oregon Green 488 conjugate	Thermo Fisher	Cat# A6374; RRID: AB_2315961
Mouse Anti-ATDC (clone H-300)	Santa Cruz	Cat# sc-376125; RRID: AB_10989362
Rabbit Anti-Cytokeratin 19 (clone H-60)	Santa Cruz	Cat# sc-25724; RRID: AB_2249714
Rabbit Anti-pan-Cytokeratin (clone H-240)	Santa Cruz	Cat# sc-15367; RRID: AB_2134438
Rat Anti-CD45 (clone 3H1363)	Santa Cruz	Cat# sc-70699; RRID: AB_1120495
Human EpCAM/TROP-1 Biotinylated Antibody	R&D Systems	Cat# BAF960; RRID: AB_356818
Chemicals, Peptides, and Recombinant Proteins		
Dextran, 250,000, Powder	Spectrum Chemical	Cat# DE130
Bovine Serum Albumin	Sigma-Aldrich	Cat# B4287
Pluronic F-127	Sigma-Aldrich	Cat# P2443
Chlorotrimethylsilane	Sigma-Aldrich	Cat# 33014
Triton X-100	Sigma-Aldrich	Cat# X100
Sodium Chloride	Thermo Fisher	Cat# S271-500
Pierce 16% Formaldehyde (w/v), Methanol-free	Thermo Fisher	Cat# 28908
PBS	Thermo Fisher	Cat# 10010-023
UltraPure™ DNase/RNase-Free Distilled Water	Thermo Fisher	Cat# 10977-015
DAPI	Thermo Fisher	Cat# D1306
ProLong Gold Antifade Mountant with DAPI	Thermo Fisher	Cat# P36931
Antibiotic-Antimycotic (100X)	Thermo Fisher	Cat# 15240062
Fetal Bovine Serum	Thermo Fisher	Cat# 10438026
Donkey Serum	Jackson Immuno	Cat# 017-000-121
Lentivirus-GFP	Vector Core at University of Michigan	N/A
Critical Commercial Assays		
MTT Cell Proliferation Assay	ATCC	Cat# 30-1010K
Arcturus PicoPure DNA Extraction Kit	Thermo Fisher	Cat# KIT0103
QIAamp DNA Micro Kit	QIAGEN	Cat# 56304
REPLI-g UltraFast Mini Kit	QIAGEN	Cat# 150033
qBiomarker Somatic Mutation PCR Array: Human Pancreatic Cancer	QIAGEN	Cat# SMH-035AA
TapeStation Genomic Tape	DNA Sequencing Core at University of Michigan	N/A
ABI 7900HT (384-well Fast Block)	DNA Sequencing Core at University of Michigan	N/A
C1 Single-Cell Reagent Kit for Preamp	Fluidigm	Cat# 100-5319
TaqMan Gene Expression Assay	Thermo Fisher	N/A

(*Continued on next page*)

Continued

REAGENT or RESOURCE	SOURCE	IDENTIFIER
Experimental Models: Cell Lines		
MCF7	ATCC	Cat# HTB-22
PANC-1	ATCC	Cat# CRL-1469
PC-3	ATCC	Cat# CRL-1435
H1650	ATCC	Cat# CRL-5883
Software and Algorithms		
R	The R Foundation	N/A
Other		
DMEM, high glucose, pyruvate	Thermo Fisher	Cat# 11995065
RPMI 1640 Medium	Thermo Fisher	Cat# 1875093

CONTACT FOR REAGENT AND RESOURCE SHARING

Further information and requests for reagents may be directed to, and will be fulfilled by the Lead Contact, Sunitha Nagrath (snagrath@umich.edu).

EXPERIMENTAL MODEL AND SUBJECT DETAILS

Cell Lines

MCF7 Cells

Cells were maintained in DMEM supplemented with 10% fetal bovine serum and 1% Antibiotic-Antimycotic (100X) at 37°C in a humidified atmosphere at 5% CO_2.

PANC-1 Cells

Cells were maintained in DMEM supplemented with 10% fetal bovine serum and 1% Antibiotic-Antimycotic (100X) at 37°C in a humidified atmosphere at 5% CO2.

PC-3 Cells

Cells were maintained in RPMI supplemented with 10% fetal bovine serum and 1% Antibiotic-Antimycotic (100X) at 37°C in a humidified atmosphere at 5% CO_2.

H1650 Cells

Cells were maintained in RPMI supplemented with 10% fetal bovine serum and 1% Antibiotic-Antimycotic (100X) at 37°C in a humidified atmosphere at 5% CO2.

Human Subjects

Informed Consent

All subjects were consented by the study team or research nurse prior to the scheduled blood draw using standard procedures for clinical research employed in the University of Michigan Comprehensive Cancer Center (UMCCC).

Control Group

Whole blood from volunteer healthy people was obtained as part of an Institutional Review Board approved protocol (HUM00070190). All participants are over 18 years of age.

Pancreatic Cancer Patients

Whole blood from patients with pancreatic cancer was obtained as part of an Institutional Review Board approved protocol (HUM00025339). All participants are over 18 years of age. Stages of disease of all subjects are listed in Table S1.

Metastatic Breast Cancer Patients

Whole blood from patients with metastatic breast cancer was obtained as part of an Institutional Review Board approved protocol (HUM00070190). All participants are over 18 years of age. Stages of disease and tumor types of all subjects are listed in Table S2.

METHOD DETAILS

Sample Preparation for Spike Cell Experiments

A pancreatic cancer cell line with green fluorescent protein (PANC-1/GFP) was cultured and mixed with white blood cells (stained with DAPI) in buffer solution (PBS). The MCF-7 breast cancer cell line was stained with Green Cell Tracker (Life Technologies) and mixed with a portion of a healthy control blood sample.

Experimental Protocol for Labyrinth

The device was pre-flowed with 1% Pluronic acid solution (diluted in 1X PBS) at 100 μL/min for 10 minutes and then incubated for 10 minutes to prevent cell clotting on channel walls. Cell sample suspended in buffer was flowed through Labyrinth at different flow rates (1000, 2000, and 3000 μL/min) and was observed under a microscope. Product from outlets was collected after 1 minute duration of flow stabilization. Waste from each outlet of Labyrinth was collected for cell counting to calculate the recovery percentage. To observe the isolation of cancer cells from other blood components, images and movies were taken using both a high-speed camera and a fluorescence microscope under brightfield, FITC, and DAPI filters.

Patient Sample Processing

Labyrinth was pre-flowed with 1% Pluronic acid solution to prevent cell clotting on channel walls. Blood samples were then processed through the device at a flow rate of 2.5mL/min.

Blood samples from pancreatic cancer patients were collected into EDTA tubes and processed through Labyrinth with 1:5 dilution with PBS, and without any further pre-processing steps. A typical run involves processing of 7.5 mL of whole blood in 15 minutes. Blood samples from metastatic breast cancer patients were collected in EDTA tubes and processed through Labyrinth within 4 hours of collection. When samples were processed to ultimately undergo downstream single cell analysis, RBCs in blood samples were removed using density separation with dextran solution (6 m/v% dextran and 0.87 m/v% sodium chloride in DNase/RNase-Free Distilled Water) prior to Labyrinth process. The blood sample with dextran solution was kept still in room temperature for 45 minutes to bring down the RBCs driven by density difference. The supernatant, which includes everything in whole blood except RBCs, was carefully taken out using pipettes, and was diluted to 25 mL with PBS.

Immunostaining Protocol of Cytoslides

Labyrinth output from outlet 2 were cytospun onto poly-lysine coated slides. Samples were permeabilized by applying 0.05% Triton X-100 (PBST) solution for 15 minutes. Slides were then blocked using 20% donkey serum for 30 minutes at room temperature (RT). A cocktail of primary antibodies were added and left in a humidified chamber overnight. The next day, cytoslides were washed thrice with 0.05% PBST for 5 minutes. Samples were incubated in the dark with secondary antibodies for 45 minutes at RT. Finally, samples were washed thrice with 0.05% PBST for 5 minutes and mounted with Prolong Gold Antifade Mountant with DAPI.

CTC Identification from Cytoslides

The immunofluorescent stained slides were auto-scanned under a Nikon TI fluorescent microscope at 10X magnification for initial assessment. A typical WBC from the slide was selected as reference for its CD45 and CK fluorescent intensity levels. A cell was identified as a WBC if it had similar CD45 and CK expression compared to the reference cell. A cell was identified as a CTC if it had at least 50% lower CD45 and 50% higher CK expression compared to the reference cell. Cells with both significant CD45 and CK expression with respect to the reference cell would be considered as double positive cells. DAPI positive cell but lower expression of CD45 and CK when compared to the reference cell were considered to be double negative cells. A scatter plot of typical CK and CD45 fluorescent intensity levels for CTC identification from patient samples is presented in Figure S3. The potential CTCs (pan-CK+/DAPI+/CD45-) were re-imaged at 40X resolution (representative images are shown in Figure 3D) to further confirm their morphology and fluorescent signals.

DNA Isolation and Mutational Analysis

DNA was extracted from five patient samples (C.1-5) using the Arcturus PicoPure DNA Extraction Kit. Extracted DNA was concentrated using the Cleanup Protocol of the QiAmp DNA Micro Kit (Qiagen). All DNA samples were amplified using the REPLI-g UltraFast Mini Kit (Qiagen) for whole genome amplification. DNA quality and quantity were measured using TapeStation Genomic Tape (DNA Sequencing Core, University of Michigan). Mutations were detected by the ABI 7900HT (384-well Fast Block) in the 384-well format (96x4) of the qBiomarker Somatic Mutation PCR Array: Human Pancreatic Cancer (Qiagen/SABiosciences). The average Ct method was used for analysis of mutations as per manufacturer recommended template.

Single Cell Multiplex Gene Expression Analysis

Cells isolated using the double Labyrinth were mixed with suspension reagent and loaded onto a C1 chip (10-17 μm) to isolate up to 96 single cells using the C1 machine (Fluidigm, USA). The loading efficiency of C1 chip for a sample containing about 1500 cells/3uL is >90%. Captured cells within the 96 chambers of the C1 chip were examined under the microscope (IX-83 Olympus, Japan) to differentiate chambers containing single cells from those with multiple cells or no cells. A typical patient sample loading onto C1 yields CTCs ranging 1-16, 10-40 WBCs and some RBCs. Then, lysis, RT and preAmplification reagents (Fluidigm and Ambion, USA) along with the pooled 96 selected TaqMan assays (Table S3, Life Technologies, USA) were added to the corresponding wells in the chip to generate preAmplified cDNAs for the 96 target genes for each single cell using the Fluidigm's STA protocol in C1 instrument. Single cell cDNA products were then subjected to qPCR using the 96 selected TaqMan assays (Life Technologies, USA), 96x96 chips, and

BioMark HD instrument (Fluidigm, USA). Results were analyzed by SINGuLAR and R script software and presented as Log2Exp in HeatMap, violin, and PCA plots.

QUANTIFICATION AND STATISTICAL ANALYSIS

Statistical parameters including the exact value of n, mean and standard deviation are reported in Figures 2 and 3, as well as in corresponding Figure Legends. Heatmap, violin plot and PCA in Figure 4 and S4 were generated using SINGuLAR Analysis Toolset (Fluidigm) in R software.